Nanotechnology Perceptions
ISSN 1660-6795
www.nano-ntp.com

Bi-Stability Analysis Of Double Diffusive Convection In A Tilted Square Porous Cavity Filled With A Non-Newtonian Power-Law Fluids

Saleh Khir[a,b,c], Rabah Henniche[c], Redha Rebhi[a,b] , Faouzi Didi[b] and Mohamed Kezrane[a,c]

[a]*Department of Mechanical Engineering, University of Medea, Medea 26000, Algeria.*
[b]*LERM-Renewable Energy and Materials Laboratory, University of Medea, Medea 26000, Algeria.*
[c]*Laboratoire de Mécanique Physique et Modélisation Mathématique (LMP2M), Université Yahia Fares de Médéa, Quartier Ain Dheb, Médéa 26000, Algérie*

Received : 25-04-2024 Accepted : 12-08-2024 Published : 26-09-2024

This research presents a numerical study of double-diffusive natural convection in a tilted square cavity with a porous layer filled with a non-Newtonian fluid. The cavity's active walls are subjected to uniform Neumann-type thermal and solute boundary conditions, involving constant heat and concentration fluxes, or Dirichlet-type conditions, with imposed constant temperature and concentration, whereas the remaining walls of the cavity are assumed to be adiabatic and impermeable. To elucidate the behavior of non-Newtonian fluids, we employed the power-law model, known as the predominant rheological model for addressing flow phenomena within porous media. The fundamental governing equations are numerically solved through the finite difference method, while the convective flow within porous media is characterized by the utilization of the Darcy model and Boussinesq approximation. The governing parameters controlling the problem include the Rayleigh number, R_T, the power-law index, n, the buoyancy ratio, N, the Lewis number, Le, and the inclination angle Φ. The results indicate that both the power-law index, n, and the inclination angle, Φ, exert notable influence on the flow intensity and the heat and mass transfer occurring through natural convection within the enclosure. Among the most fascinating findings of this research is the recognition of a phenomenon termed bi-stability, which signifies the presence of two stable solutions.

Keywords: Double-diffusive convection, bi-stability phenomenon,power-law fluids, inclined porous layer.

I. INTRODUCTION

Double-diffusive convection is a fascinating phenomenon in fluid dynamics where heat and mass transfer occur simultaneously due to gradients in temperature and concentration. When

this process takes place within a porous medium, the interplay between the fluid flow and the solid matrix significantly influences the overall heat and mass transport characteristics. In many practical applications environmental, industrial, and geophysical, the working fluids exhibit non-Newtonian behavior, meaning their viscosity is not constant but shear-rate dependent. This introduces additional complexities compared to Newtonian fluids [1-3].

A brief examination of the literature on the natural convection of Newtonian fluids in square cavities led to the discovery of a number of intriguing and practical recent findings that have improved our understanding of these processes in a variety of fluid systems.Ozu and Sayama [4] conducted experimental and numerical studies on natural convection in an inclined square channel with uniform temperatures on opposing sides. Their findings indicate that maximum heat transfer occurs at a 50-degree inclination, while minimum heat transfer and a change in flow pattern occur at a 10-degree inclination. Both methods produced consistent Nusselt number values. Saeid, et al [5] investigated numerically the natural convection in a square cavity filled with a porous medium using the non-Darcy model, showing how increasing the inertial effects parameter slows down convection currents and reduces the average Nusselt number for constant Rayleigh numbers. A numerical analysis of unsteady 2-D natural convection under magnetic influence in a laterally and volumetrically heated square cavity was given by Sarris et al. [6] The study demonstrated transitions between steady and unsteady flow patterns with different internal Rayleigh numbers and the Hartmann number. Pirmohammadi and Ghassemi [7] investigated numerically a natural convection in a tilted enclosure with a magnetic field, their findings indicated that increased Hartmann numbers lead to a reduction in convective heat transfer. They further demonstrated the impact of inclination angle on the Nusselt number at Ra=10^4 and 10^5, noting a peak around φ=45°.The impact of magnetic field strength on fluid flow and heat transfer in a hollow with inclined sides was studied numerically by Revnic et al. [8]. Their findings highlight changes in streamlines and isotherms due to the magnetic field. The study examines how the magnetic field affects flow patterns, temperature distribution, and heat transfer characteristics within the cavity, offering insights into the convective behavior under different conditions. Costa et al. [9] investigated the influence of a magnetic field induced by dual vertical electric currents on natural convection within square enclosures filled with fluid-saturated porous media. Their study reveals that increasing the magnetic field strength results in a decrease in convection intensity. Consequently, the generated magnetic field consistently diminishes natural convection within the enclosure, thereby reducing the overall heat transfer across it. Recently, Rebhi et al. [10] conducted a numerical investigation on double-diffusive convection within an inclined square porous cavity under a magnetic field. Their study revealed that the natural convection heat and mass transport within the porous layer are significantly impacted by both the magnetic field and the inertial effect parameter. Alilat et al. [11] numerically study the natural convection in an inclined porous square enclosure filled with Cu-water nanofluid, the Darcy-Dupuit model, which includes the inertial effects parameter, describes the flow in the porous medium., highlighting that increased inertial effects reduce convection intensity while higher nanoparticle volume fraction and porosity impact heat transfer differently. An optimal cavity inclination of around 40° maximizes convection.

In the context of non-Newtonian,Numerous numerical investigations have examined flows in such configuration. Beghein et al. [12] investigated various solutal Rayleigh numbers and Lewis numbers in Thermosolutal convection inside a square cavity. They looked at the connections between the mass and heat transfer rates in various flow configurations that were powered by heat or mass.Wang et al. [13] investigate natural convection of non-Newtonian power-law fluids over permeable bodies within a porous medium. The study analyzes the effects of yield stress, permeability constant, and power-law index on heat flux, wall temperature, lateral mass flux, and boundary heat flux, revealing significant dependencies on these parameters. It was found that natural convection initiates only if a minimum yield stress value is present. Ohta et al. [14] employ the Sutterby model to analyze natural convection of pseudoplastic fluids within a square cavity. Their findings reveal that shear-thinning enhances heat transfer relative to Newtonian fluids by decreasing apparent viscosity near the walls. However, high pseudoplasticity combined with increased Rayleigh numbers can result in complex flow fields. Jecl and Škerget. [15] examine the application of the Boundary Element Method (BEM) for analyzing natural convection in a square porous cavity filled with non-Newtonian fluids, incorporating various viscosity models such as the power-law and Carreau models. They compare their findings with those obtained using the finite difference method, demonstrating both good agreement between the two approaches and the efficiency of BEM in addressing transport phenomena in porous media. Turan et al. [16] conduct a simulation of laminar natural convection in square enclosures filled with power-law fluids, showing that Nusselt number increases with Rayleigh number for both Newtonian and power-law fluids. The study reveals that shear-thinning fluids ($n < 1$) enhance convective heat transfer, whereas shear-thickening fluids ($n>1$) diminish it. The authors provide a detailed analysis and propose new correlations for Nu based on Ra, Prandtl number (Pr), and the power-law index (n). Using the finite volume method, Vinogradov et al. [17] numerically investigate steady natural convection in cavities filled with non-Newtonian shear-thickening fluids that are heated from below and cooled from above. Although the heat transfer rates across the two fluid types varied, the study indicates that both Newtonian and non-Newtonian fluids display similar heat transfer behavior and transitions in flow structure with various inclination angles. In their study of MHD natural convection in a square differentially heated porous cavity, Ahmed et al. [18] considered the effects of radiation and viscous dissipation. It has been demonstrated that conductive heat transfer intensifies with an increase in the radiation parameter. It has been discovered that the average Nusselt number increases as the radiation parameter increases.Kefayati [19] employs the Finite Difference Lattice Boltzmann Method (FDLBM) to analyze natural convection of power-law non-Newtonian molten polymers in a cavity with a sinusoidally heated wall. The study reveals that higher power-law indices generally diminish heat transfer, with the impact of the power-law index being more significant at a Rayleigh number ($Ra=10^5$) compared to ($Ra=10^4$), though the variation is minimal.Astanina et al. [20,21] have quantitatively studied transient natural convection in a non-Darcy porous cavity with temperature-dependent viscosity. They found that increasing the viscosity variation parameter intensifies convective flow and heat transfer, forming a single-core convective cell within the cavity. Additionally, their investigation into the effects of natural convection and thermal radiation using finite difference methods revealed that increasing the radiation parameter ($0 \leq Rd \leq 10$), Darcy number ($10^{-5} \leq Da \leq 10^{-2}$), and viscosity variation parameter

($0 \leq C \leq 6$) significantly enhances convective flow.Raisi [22] conducts a numerical investigation into natural convection heat transfer within a square enclosure containing fixed temperature baffles on the left wall, filled with a power-law non-Newtonian fluid. Utilizing the finite difference method and the SIMPLE algorithm, the study examines the effects of Rayleigh number, power-law index, baffle length, and baffle spacing on flow, temperature fields, and heat transfer. The results indicate that an increased Rayleigh number enhances heat transfer, particularly for fluids with lower power-law indices.Makayssi et al. [23] investigate heat and mass transfer via natural convection in a square cavity filled with shear-thinning non-Newtonian binary fluids, employing the Carreau model. By applying Dirichlet thermal and solutal boundary conditions on the vertical walls, the study numerically examines the effects of the thermal Rayleigh number and Prandtl number on fluid behavior. Lounis et al. [24] conduct an investigation into Thermosolutal convection of non-Newtonian fluids within an inclined square enclosure. Employing a Carreau-Yasuda model, the study delves into the influence of diverse rheological and thermophysical parameters. Numerical results indicate that augmenting the time constant parameter enhances both thermal and mass exchange, whereas reducing the viscosity ratio and parameter a heightens both transfers. Notably, altering the inclination angle shows no discernible pattern in its impact. Double-diffusive convection in a square cavity with a porous layer saturated with shear-thinning non-Newtonian fluid is investigated by Ould Larbi et al. [25]. Using the finite difference method and the Carreau-Yasuda rheological model, the study clarifies the significant impact of shear behavior on heat and mass transfer processes. The results show that conduction gives way to convection as the buoyancy ratio increases, with mass and heat transfer being most advantageous at a 45° inclination angle.

As a continuation of the numerical simulation series conducted by Khir et al. [26,27], this study offers a comprehensive numerical investigation of double-diffusive convection in an inclined square porous cavity filled with a non-Newtonian fluid. The behavior of non-Newtonian fluids is characterized using the power-law model. The walls of the active cavity are subjected to either Dirichlet boundary conditions, which impose constant temperature and concentration, or uniform Neumann boundary conditions, which involve constant heat and solute fluxes. The system of governing equations is numerically solved using the time-accurate finite difference method. The results are given as a function of heat transfer rate, mass transfer rate, and flow intensity, and their dependency on the governing parameters is analyzed in detail. One of the most interesting findings of the research is the identification of bi-stability, indicating the presence of two stable solutions under both Dirichlet-type and Neumann-type boundary conditions.

II. PROBLEM DEFINITION AND MATHEMATICAL FORMULATION

In the current investigation, Figure 1 represent a two-dimensional square cavity filled with a non-Newtonian power-law fluid-saturated porous media, with dimensions specified by $L' \times H'$. The horizontal and vertical orientations of the coordinate axes x' and y' are aligned at an angle Φ. The active cavity walls are considered to be uniformly subjected to either Dirichlet-type conditions, with constant temperature T' and concentration S', or Neumann-

type thermal and solute boundary conditions, with constant heat q′ and solute j′ fluxes. The remaining cavity walls are considered to be adiabatic and impermeable.

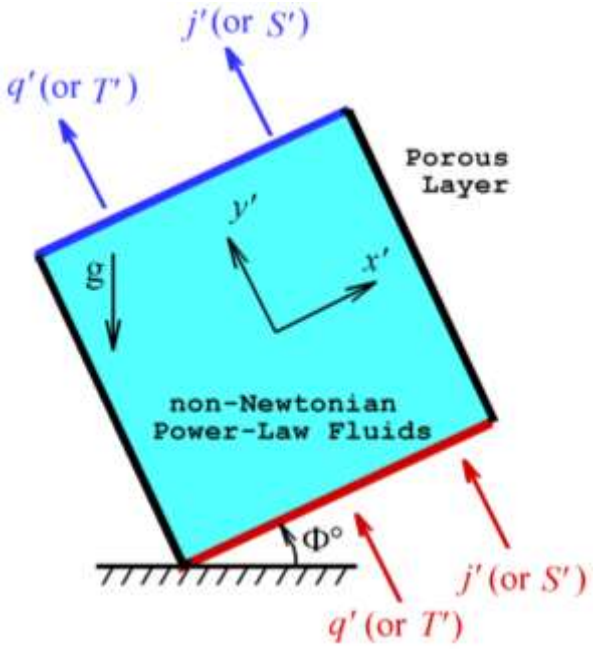

Figure 1. Sketch of the cavity's coordinate system and boundary conditions.

The simulation of the flow employs the power-law model and the Boussinesq approximation, where the fluid density correlates linearly with changes in temperature and solute concentration, as follows:

$$\rho = \rho_0 \left[1 - \beta_T' \left(T' - T_0'\right) - \beta_S' \left(S' - S_0'\right)\right] \tag{1}$$

The terms ρ_0, β_T, and β_S denote the fluid mixture density at the reference temperature $T' = T_0$ and solute fraction $S' = S_0$, as well as the thermal and concentration expansion coefficients, respectively. Here, the subscript 0 signifies the reference state at the coordinate system's origin.

The expression delineating the laminar flow of a non-Newtonian power-law fluid through a porous medium is expressed as follows:

$$\vec{V}' = -\frac{K}{\mu_a'} \nabla p' \tag{2}$$

Where

$$\mu_a' = \varepsilon\left(u'^2 + v'^2\right)^{(n-1)/2} \tag{3}$$

$$\varepsilon = \frac{2h}{8^{(n+1)/2}\left(K\phi\right)^{(n-1)/2}\left(n/\left(1+3n\right)\right)^n} \tag{4}$$

Herein,ϕ and K denote the porosity and permeability of the porous medium, respectively, whileV′ represents the superficial velocity. The term μ'_arefers to the apparent viscosity, where h represents the consistency index and ndenotes the power-law index.

For the present situation, the following equations describe the conservation of mass, momentum, energy, and concentration:

$$\nabla.\vec{V'} = 0 \tag{5}$$

$$\vec{V}' = -\frac{K}{\mu_a'}\left[\nabla p' + \rho_0 \vec{g}\left[1-\beta_T'\left(T'-T_0'\right)-\beta_S'\left(S'-S_0'\right)\right]\right] \tag{6}$$

$$\left(\rho C\right)_p \frac{\partial T'}{\partial t'} + \left(\rho C\right)_f J(\Psi', T') = k\nabla^2 T' \tag{7}$$

$$\phi\frac{\partial S'}{\partial t'} + J(\Psi', S') = D\nabla^2 S' \tag{8}$$

$(\rho C)_f$and $(\rho C)_p$are the heat capacities of fluid and saturated porous medium, whereg is the gravitationalacceleration.

Equations (5)-(8) are put in a dimensionless form by defining a new set of variables

$$\begin{gathered}(x,y) = (x',y')/H' \quad (u,v) = (u',v')H'/\alpha \quad t = t'\alpha/\left(\sigma H'^2\right) \\ \psi = \psi'/\alpha \quad T = \left(T'-T_0'\right)/\Delta T' \quad \Delta T' = q'H'/k \\ S = S'/\Delta S' \qquad \Delta S' = j'/\rho D \quad \mu_a = h/\varepsilon\left(\alpha/H'\right)^{n-1}\end{gathered} \tag{9}$$

Where $\alpha = k/(\rho C)_f$ is the thermal diffusion coefficient, and $\sigma = (qC)_p/(qC)_f$ is the heat capacity ratio.

By applying the previously mentioned equations and removing the pressure term from Equation (5), the dimensionless equations controlling the convective flow are shown below:

$$\nabla^2\Psi = -\mu_a^{-1}\left[\frac{\partial\Psi}{\partial y}\frac{\partial\mu_a}{\partial y} + \frac{\partial\Psi}{\partial x}\frac{\partial\mu_a}{\partial x} + R_T\left(\left(\frac{\partial T}{\partial x} + N\frac{\partial S}{\partial x}\right)\cos\Phi - \left(\frac{\partial T}{\partial y} + N\frac{\partial S}{\partial y}\right)\sin\Phi\right)\right] \tag{10}$$

$$\nabla^2 T = \frac{\partial T}{\partial t} + \frac{\partial\Psi}{\partial y}\frac{\partial T}{\partial x} - \frac{\partial\Psi}{\partial x}\frac{\partial T}{\partial y} \tag{11}$$

$$Le^{-1}\nabla^2 S = \xi\frac{\partial S}{\partial t} + \frac{\partial \Psi}{\partial y}\frac{\partial S}{\partial x} - \frac{\partial \Psi}{\partial x}\frac{\partial S}{\partial y} \tag{12}$$

$$\mu_a = \left[\left(\frac{\partial \Psi}{\partial x}\right)^2 + \left(\frac{\partial \Psi}{\partial y}\right)^2\right]^{\frac{n-1}{2}} \tag{13}$$

From Eqs. (10)-(13),various controlling parameters are evident, namely: Rayleigh number R_T, the Lewis number Le, the buoyancy ratio N, the normalized porosity ξ.

$$R_T = \frac{K\rho g \beta_T' \Delta T' \left(H'/\alpha\right)^n}{\varepsilon}, \quad Le = \frac{\alpha}{D}, \quad N = \frac{\beta_S' \Delta S'}{\beta_T' \Delta T'}, \quad \text{and} \quad \xi = \frac{\phi}{\sigma} \tag{14}$$

The dimensionless stream function Ψ defined as

$$u = \frac{\partial \Psi}{dy}, \quad v = -\frac{\partial \Psi}{dx} \tag{15}$$

The hydrodynamic boundary conditions applied on the system's walls are expressed in dimensionless form as follows:

$$v = \Psi = 0 \quad \text{at} \quad x = \pm\frac{1}{2}, \quad \text{and} \quad u = \Psi = 0 \quad \text{at} \quad y = \pm\frac{1}{2} \tag{16}$$

The thermal and solutal boundary conditions for constant heat and solute fluxes, known as Neumann type, are as follows:

$$\frac{\partial T}{\partial x} = \frac{\partial S}{\partial x} = 0 \quad \text{at} \quad x = \pm\frac{1}{2}, \quad \text{and} \quad \frac{\partial T}{\partial y} = \frac{\partial S}{\partial y} = -1 \quad \text{at} \quad y = \pm\frac{1}{2} \tag{17}$$

for constant temperature and concentration (Dirichlet type) are given by:

$$T = S = \pm\frac{1}{2} \quad \text{at} \quad y = \pm\frac{1}{2} \tag{18}$$

The local and average Nusselt and Sherwood numbers, denoted as Nu_x, Nu_m, Sh_x, and Sh_m, respectively, are given by:

$$\left.\begin{aligned} Nu_x &= \frac{1}{T_{(x,-1/2)} - T_{(x,1/2)}} \quad ; \quad Sh_x = \frac{1}{S_{(x,-1/2)} - S_{(x,1/2)}} \quad \text{(Neumann)} \\ Nu_x &= -\left.\frac{\partial T}{\partial y}\right|_{y=\pm 1/2} \quad ; \quad Sh_x = -\left.\frac{\partial S}{\partial y}\right|_{y=\pm 1/2} \quad \text{(Dirichlet)} \\ Nu_m &= \int_{-1/2}^{+1/2} Nu_x dx \quad ; \quad Sh_m = \int_{-1/2}^{+1/2} Sh_x dx \end{aligned}\right\} \tag{19}$$

III. NUMERICAL SOLUTION

The finite difference method with a uniform grid size is utilized to numerically solve the governing equations (10)-(12) and the boundary conditions equations (16)-(18). A second-order centered technique is used to discretize the energy and concentration equations. Two tri-diagonal matrix systems are produced for resolution at each time increment using Peaceman and Rachford's alternating directions implicit method (ADI) [28]. One of these matrix systems results from implicit discretization in the x-direction, while the other comes from implicit discretization in the y-direction. The over relaxation method (S.O.R.) was utilized to solve the momentum equation, Eq. (10). Considering steady-state solutions, convergence is achieved when the following equation is satisfied:

$$\frac{\sum_i \sum_j \left|\Psi_{i,j}^{k+1} - \Psi_{i,j}^{k}\right|}{\sum_i \sum_j \left|\Psi_{i,j}^{k}\right|} \leq 10^{-6} \tag{20}$$

In this context, $\Psi_{i,j}^{k}$ represents the stream function value at the node (i,j) in the k^t iteration. According to convergence tests, a 200x200 grid is sufficient to correctly reproduce convective flow and minimize calculation time. These findings, which are displayed in Table 1, have various values of mesh sizes: 50 x 50, 100 x 100, 150 x 150, 200 x 200, and 250 x 250.

Table 1. Convergence tests for specified parameters, $A = 1$, $Le = 5$, $N = -0.1$, $R_T = 100$, and $\Phi = 0°$, and different power-law index,n, With Neumann-type boundary conditions.

	Numerical solution					
Grids		50x50	100x100	150x150	200x200	250x250
$\boldsymbol{n = 0.6}$	Ψ_0	5.267	5.260	5.240	5.235	5.232
	Nu	4.789	4.787	4.784	4.783	4.783
	Sh	9.732	9.716	9.700	9.692	9.688
$\boldsymbol{n = 1.0}$	Ψ_0	3.146	3.145	3.145	3.145	3.145
	Nu	2.929	2.929	2.928	2.928	2.928
	Sh	7.397	7.386	7.380	7.377	7.376
$\boldsymbol{n = 1.4}$	Ψ_0	2.128	2.102	2.078	2.069	2.064

Nu	1.904	1.902	1.898	1.897	1.897
Sh	5.785	5.779	5.776	5.775	5.775

The streamlines, Ψ, temperature, T, concentration, S, and apparent viscosity, μ_a, computed numerically for $R_T = 100$, $Le = 5$, and $N = -0.1$, across different values of the power-law index, n (0.6, 1.0, and 1.4), are depicted in Figure 2, and Figure 3 under Neumann-type and Dirichlet-type boundary conditions, respectively. The impact of the power-law index, n, under Neumann-type boundary conditions as depicted in Figure 2 reveals a uniform distribution of streamlines with designated increments, $\Delta\Psi$, reaching its highest value, Ψ_{max}, near the center and ending at zero at the borders. Moreover, the increase in the power-law index, n, from $n = 0.6$ to $n = 1.4$ substantially diminishes the intensity of convective motion within the porous layer, as evidenced by the stream function value at the cavity's center: $\Psi_0 = 5.235$ for $n = 0.6$, $\Psi_0 = 3.145$ for $n = 1.0$, and $\Psi_0 = 2.069$ for $n = 1.4$. The isotherms and iso-concentration lines, which exhibit less distortion, suggest that heat and mass transfer tend towards diffusive behavior. Consequently, as depicted in Figure 2, both temperature and concentration gradients are significantly suppressed with an increase in n, leading to the emergence of parallel constant temperature and concentration lines. For instance, at these conditions, $Nu = 4.783$ and $Sh = 9.699$ for $n = 0.6$, $Nu = 2.929$ and $Sh = 7.380$ for $n = 1.0$, and $Nu = 1.897$ and Sh=5.776 for $n = 1.4$. The

apparent viscosity, μ_a, lines exhibit a consistent distribution from the center, where $\mu_a = 11.909$ for $n = 0.6$, $\mu_a = 1.000$ for $n = 1.0$, and $\mu_a = 0.132$ for $n = 1.4$, to the cavity edges.

Figure 2. Contours of streamlines, Ψ, Temperature, T, Concentration, S, and apparent viscosity, μ_a, for $R_T = 100$, $Le = 5$, $N = -0.1$ and various values of n, with Neumann-type boundary conditions.

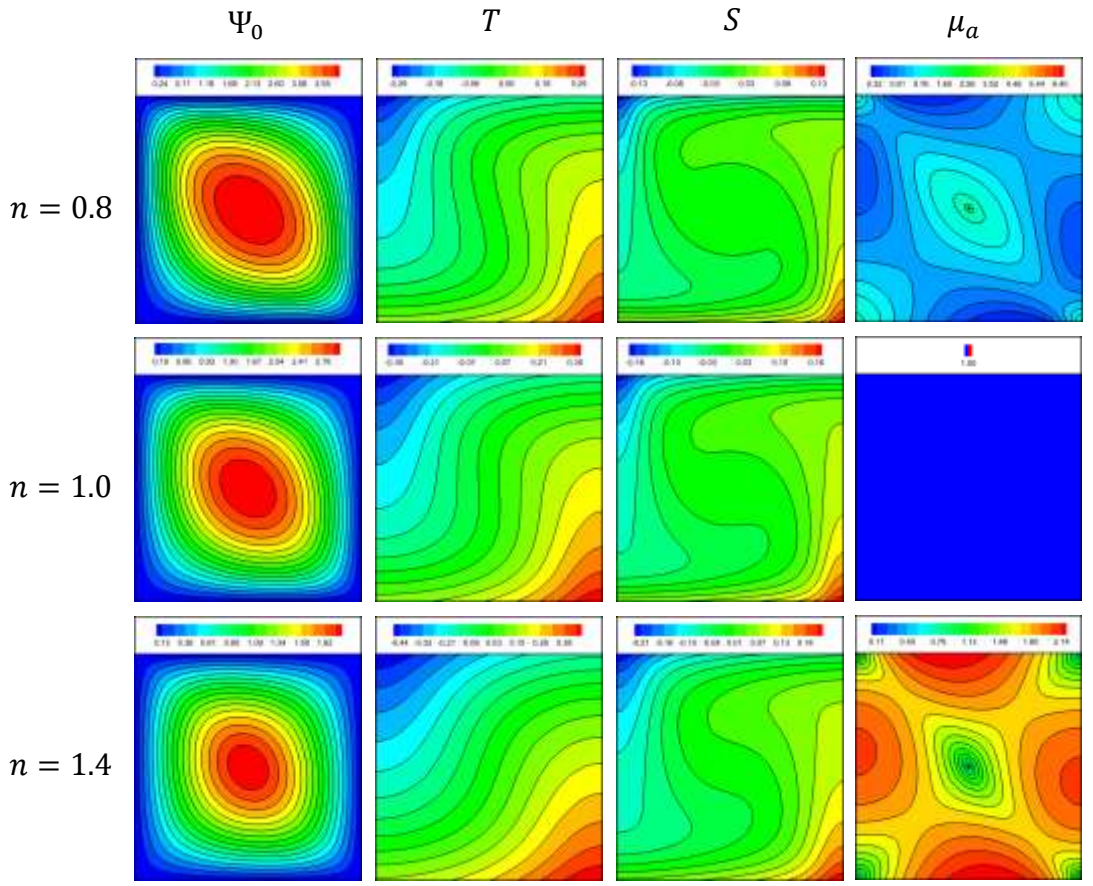

Figure 3 presents similar results to Figure 2, showcasing streamlines, Ψ, temperature, T, concentration, S, and apparent viscosity, μ_a. However, it's notable that when applying Neumann boundary conditions, the values of stream function, temperature, concentration, and apparent viscosity are lower compared to applying Dirichlet boundaries. For instance, for $n = 0.6$, $\Psi_0 = 12.766$, $Nu = 5.946$,$Sh = 12.955$, and $\mu_a = 10.761$; for $n = 1.0$, $\Psi_0 = 5.123$, $Nu = 2.736$,$Sh = 6.445$, and $\mu_a = 1.000$; and for $n = 1.4$, $\Psi_0 = 2.016$, $Nu = 1.371$,$Sh = 3.442$, and $\mu_a = 0.037$.

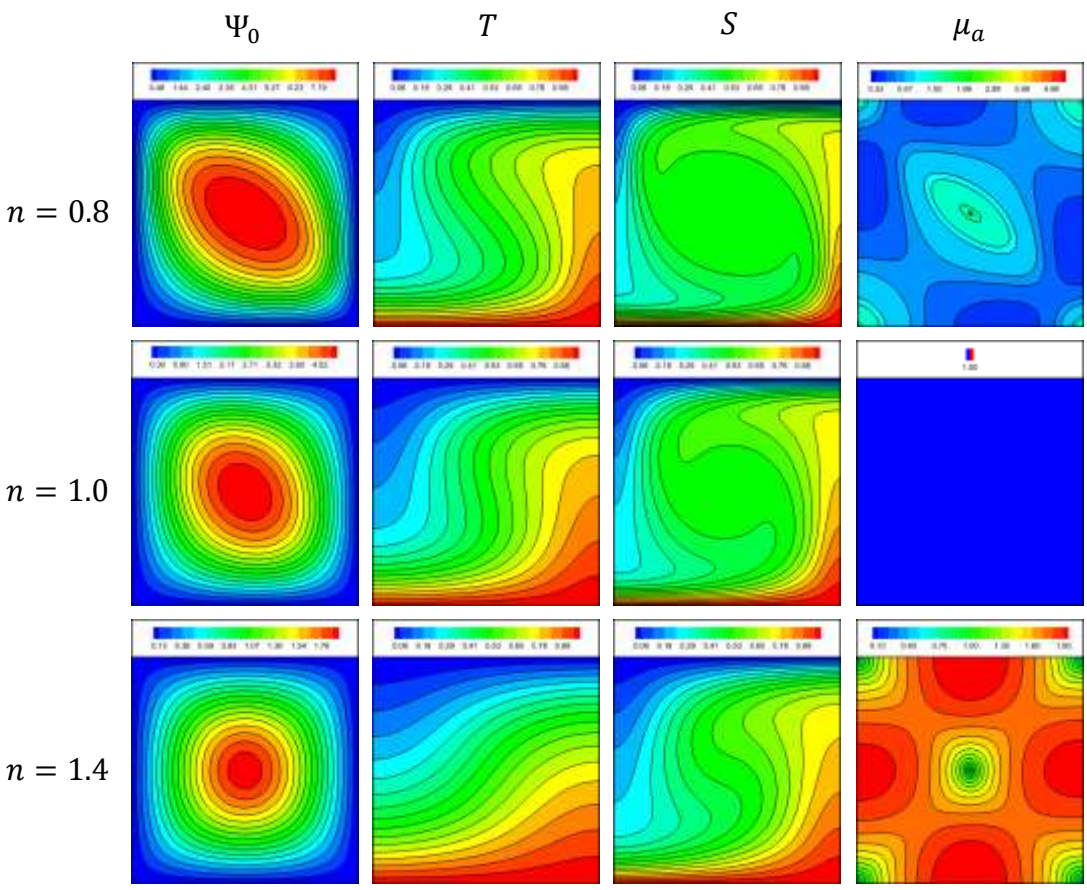

Figure 3. Contours of streamlines, Ψ, Temperature, T, Concentration, S, and apparent viscosity, μ_a, for $R_T = 100$, $Le = 5$, $N = -0.1$ and various values of n, with Dirichlet-type boundary conditions.

Figures 4 and 5 portray the numerically computed streamlines, Ψ, temperature, T, concentration, S, and apparent viscosity, μ_a, for $R_T = 100$, $Le = 5$, $N = -0.1$, and $n = 1.2$, spanning various inclination angles, Φ, from 0° to 180°. These figures illustrate the influence of Φ under both Neumann-type and Dirichlet-type boundary conditions, showcasing consistent trends in the contours of stream function, temperature, concentration, and apparent viscosity.The streamlines exhibit a uniform distribution with specified increments, $\Delta\Psi$, peaking at its maximum value, Ψ_{max}, near the center and diminishing to zero at the perimeters. Additionally, an increase in the inclination angle, Φ, notably reduces the intensity of convective motion within the porous layer, indicated by the stream function value at the center of the cavity: $\Psi_0 = 2.668$ for $\Phi = 40°$, $\Psi_0 = 2.181$ for $\Phi = 80°$, and $\Psi_0 = 1.361$ for $\Phi = 120°$ under Neumann-type boundary conditions, and $\Psi_0 = 4.363$ for $\Phi = 40°$, $\Psi_0 = 3.703$ for $\Phi = 80°$, and $\Psi_0 = 2.211$ for $\Phi = 120°$ under Dirichlet-type boundary conditions. The isotherms and iso-concentration lines display a uniform distribution between the maximum temperature, T_{max}, and the minimum temperature, T_{min}, as well as between the maximum

concentration, S_{max}, and the minimum concentration, S_{min}. Consequently, both temperature and concentration gradients are notably attenuated with an increase in Φ. For example, under these circumstances, the Nusselt number, Nu, and Sherwood number, Sh, take specific values: under Neumann-type boundary conditions $Nu = 2.679$ and $Sh = 7.882$ for $\Phi = 40°$, $Nu = 2.328$ and $Sh = 7.829$ for $\Phi = 80°$, and $Nu = 1.594$ and $Sh = 6.242$ for $\Phi = 120°$. Similarly, under Dirichlet boundary conditions, these values are: $Nu = 2.124$ and $Sh = 5.354$ for $\Phi = 40°$, $Nu = 1.800$ and $Sh = 4.824$ for $\Phi = 80°$, and$Nu = 1.334$ and $Sh = 3.681$ for $\Phi = 120°$.The apparent viscosity, represented by $\mu_a$lines, displays a uniform distribution from the center to the cavity edges. Specifically, μ_a values are observed to be 0.312 for $\Phi = 40°$, 0.230 for $\Phi = 80°$, and 0.132 for $\Phi = 120°$ under Neumann-type boundary conditions, and for a Dirichlet boundary conditions $\mu_a = 0.205$ for $\Phi = 40°$, $\mu_a = 0.439$ for $\Phi = 80°$, and $\mu_a = 0.332$ for $\Phi = 120°$. However, it is noteworthy that when applying Neumann boundary conditions, the stream function and the apparent viscosity values are lower compared to when using Dirichlet boundaries, The converse holds for the temperature and concentration

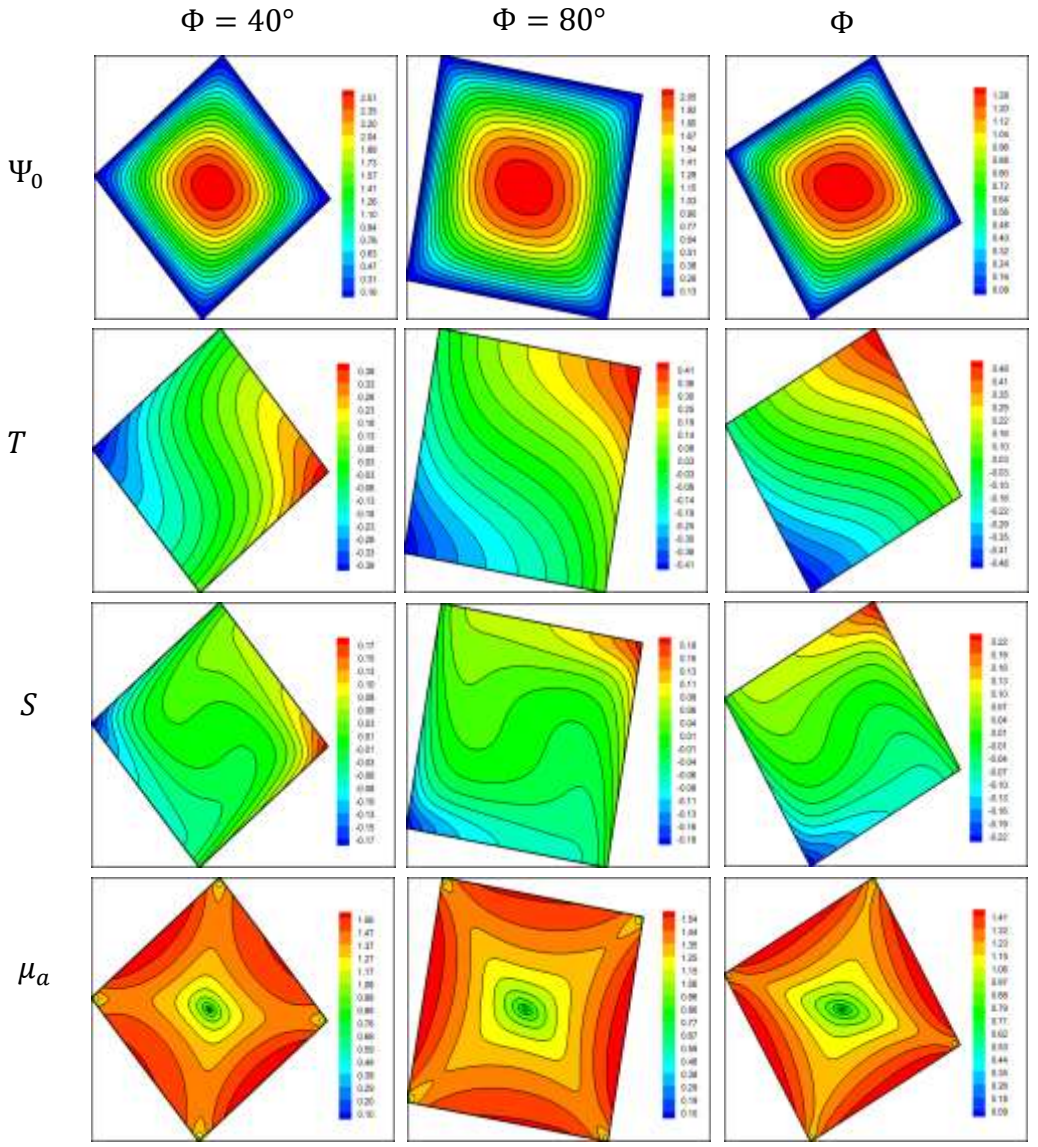

Figure 4. Contours of streamlines, Ψ, Temperature, T, Concentration, S, and apparent viscosity, μ_a, for $R_T = 100$, $Le = 5$, $N = -0.1$, $n = 1.2$ and various values of Φ, with Neumann-type boundary conditions.

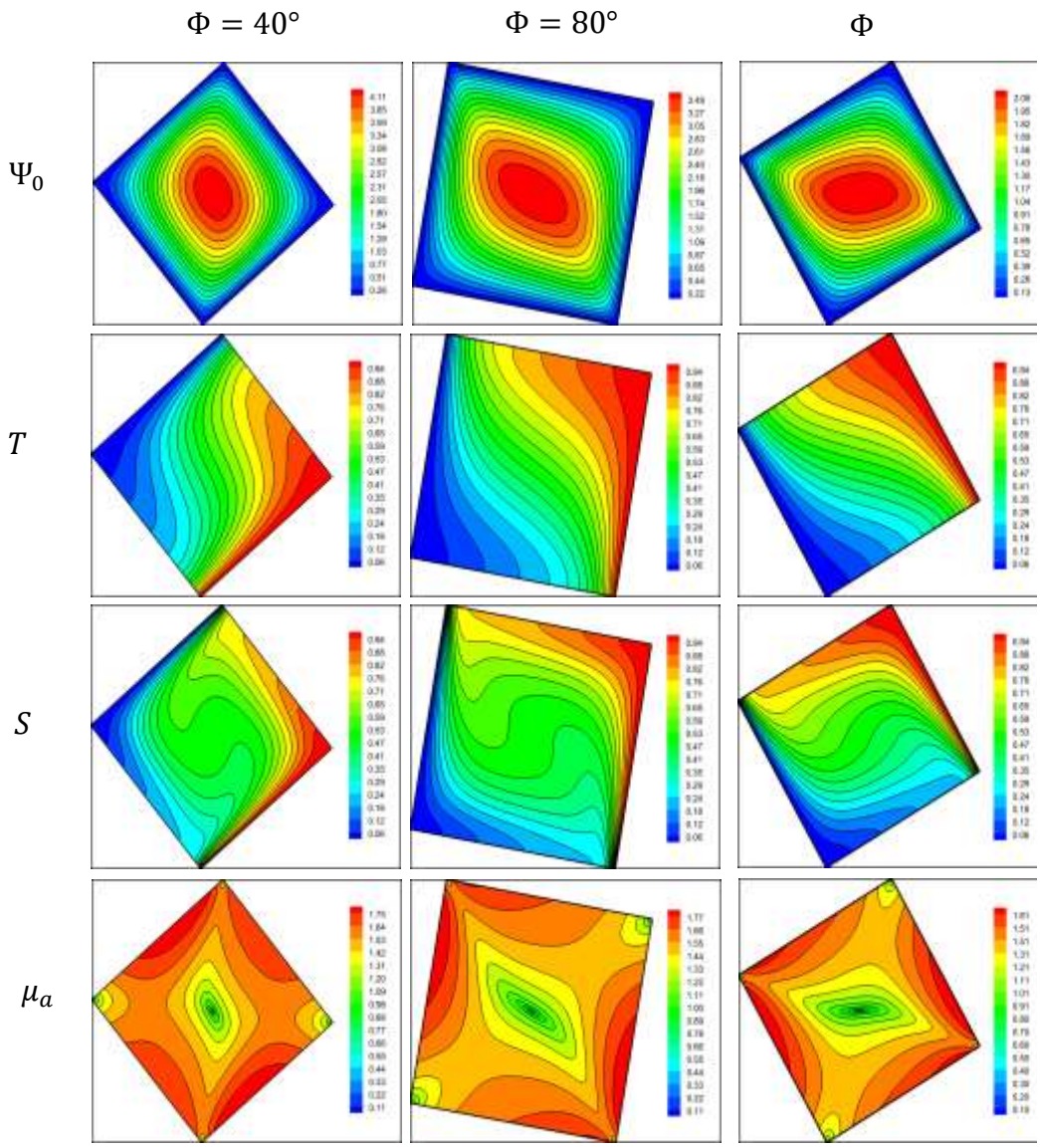

Figure 5. Contours of streamlines, Ψ, Temperature, T, Concentration, S, and apparent viscosity, μ_a, for $R_T = 100$, $Le = 5$, $N = -0.1$, $n = 1.2$ and various values of Φ, with Dirichlet-type boundary conditions.

V. RESULTS AND DISCUSSION

In this work, the impact of the power-law index, n, the Rayleigh number, R_T, the buoyancy ratio, N, the Lewis number, Le, and the angle of inclination Φ on the behaviors of heat and mass transfer, bistability convective flows, and square porous cavities is being examined. The numerical results presented in this study encompass the ranges $0.6 \leq n \leq 1.4$, $0 \leq \Phi \leq 180°$, and $-5 \leq N \leq 5$. Since the bifurcation onset is of relevance, we take into account comparatively small values of the Rayleigh number, $R_T \leq 200$, aroundthe critical sites. Additionally, Dirichlet and Neumann boundary conditions are taken into consideration to extend the circumstances under which bi-stability convection may occur and guarantee the existence of bi-stability convection for any kind of thermal and solutal boundary condition.

Figure 6(1)-(2) presents the numerical results of the profiles of the horizontal velocity, U, the apparent viscosity, μ_a, temperature, T, and concentration, S, under both Neumann-type (left) and Dirichlet-type (right) boundary conditions, obtained at the center of the cavity ($x = 0$), for different values of power-law index, n, respectively. For: $R_T = 100$, $N = -0.1$, $Le = 5$, and $\Phi = 0°$. As shown in Figure. 6(1.a), the horizontal velocity increases with the decrease in the power-law index, n, while the fluid becomes increasingly shear-thinning. Furthermore, it's worth mentioning that the horizontal velocity,U, is more prominent at the cavity border and absent in the central area. Notably, in the case of a Newtonian fluid, the velocity distribution adheres to a linear configuration.

The representation of apparent viscosity in Figure 6(1.b) illustrates a declining pattern as the power-law index, n, decreases. This indicates a decrease in the prominence of convective motion when the fluid demonstrates shear-thickening behavior ($n > 1$). Conversely, contrasting effects are noted for shear-thinning fluids ($n < 1$), while it remains consistently constant ($\mu_a = 1$) for Newtonian fluids ($n = 1$).

Figure 6(1.c) illustrates that with a decrease in the power index, n, the temperature between the horizontal walls diminishes, leading to a notable rise in the convective heat transfer rate, represented by the Nusselt number. This trend is similarly observed in the concentration profiles depicted in Figure 6(1.d). It's noted that the disparity in concentration between the two horizontal walls diminishes significantly, enhancing mass transfer, represented by the Sherwood number.

Under Dirichlet-type boundary conditions Figure 6(2.a)-(2.d), with certain distinctions worth mentioning. Notably, the values of the horizontal velocity U, apparent viscosity μ_a, temperature T, and concentration S under Neumann-type boundary conditions are lower compared to those under Dirichlet-type boundary conditions. The temperature and concentration values are set to 1 at the bottom wall of the cavity, in accordance with adherence conditions.

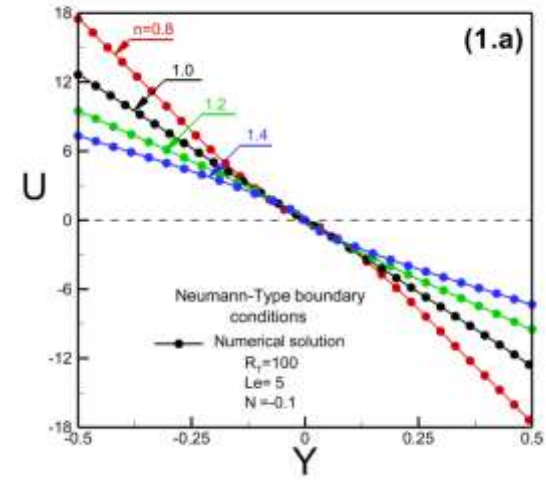
(1.a)
n=0.8
1.0
1.2
1.4
U
Y
Neumann-Type boundary conditions
Numerical solution
R_t=100
Le= 5
N =-0.1

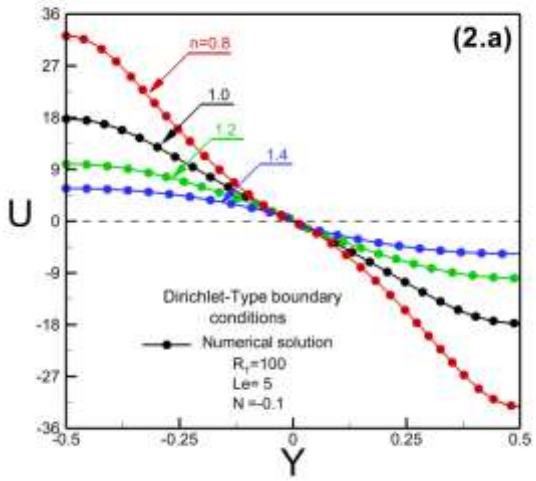
(2.a)
n=0.8
1.0
1.2
1.4
U
Y
Dirichlet-Type boundary conditions
Numerical solution
R_t=100
Le= 5
N =-0.1

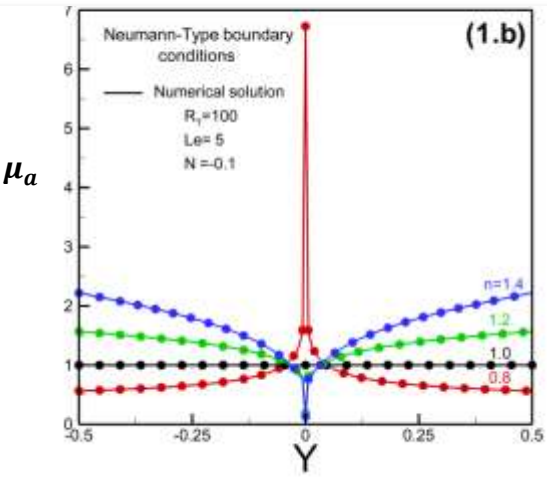
(1.b)
μ_a
Y
Neumann-Type boundary conditions
Numerical solution
R_t=100
Le= 5
N =-0.1
n=1.4
1.2
1.0
0.8

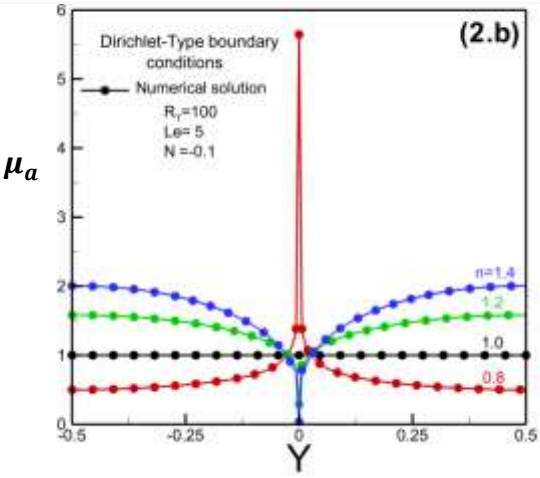
(2.b)
μ_a
Y
Dirichlet-Type boundary conditions
Numerical solution
R_t=100
Le= 5
N =-0.1
n=1.4
1.2
1.0
0.8

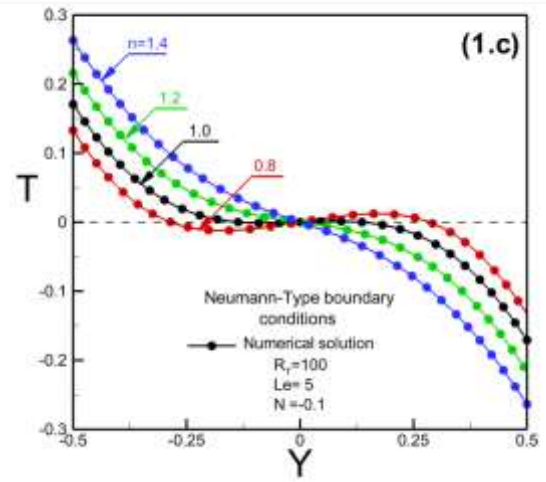
(1.c)
n=1.4
1.2
1.0
0.8
T
Y
Neumann-Type boundary conditions
Numerical solution
R_t=100
Le= 5
N =-0.1

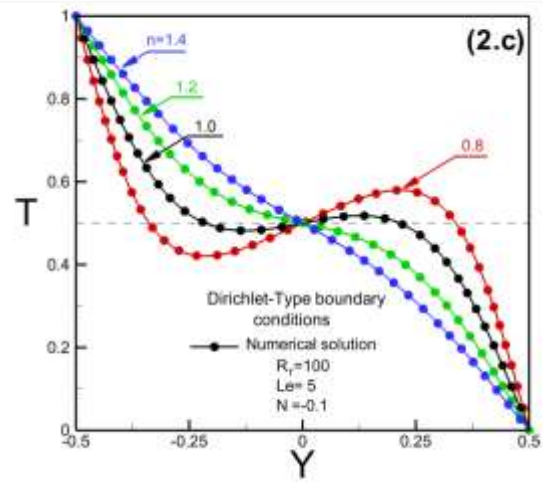
(2.c)
n=1.4
1.2
1.0
0.8
T
Y
Dirichlet-Type boundary conditions
Numerical solution
R_t=100
Le= 5
N =-0.1

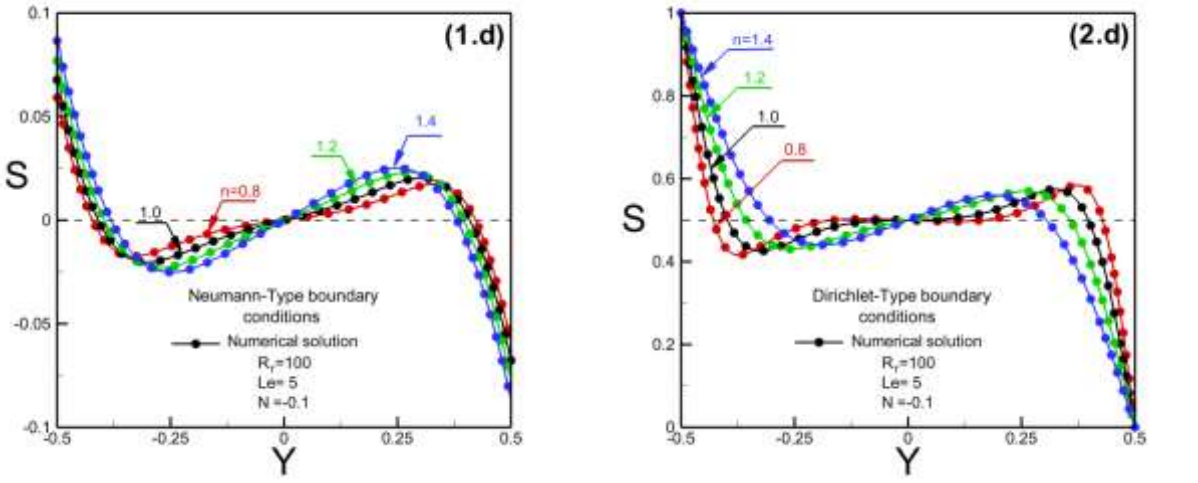

Figure 6. Effect of the power-law index, n, on the profiles of (a) the horizontal velocity, U, (b) apparent viscosity, μ_a, (c) temperature, T, and (d) concentration, S, under both Neumann-type (left) and Dirichlet-type (right) boundary conditions.

Figures7(1)-(2) illustrates the impact of the inclination angle, Φ, on the intensity of flow, Ψ_0, the Nusselt number, Nu, and the Sherwood number, Sh, under both Neumann-type (left) and Dirichlet-type (right) boundary conditions. The investigation is conducted for $R_T = 100$, $Le = 5$, $N = -0.1$, and varying values of the power-law index, n. The curves depicted in the graphs represent the predictions of the current numerical nonlinear models. The results brightly demonstrate that Φ profoundly influences the strength of convection and subsequent heat and mass transfer. It is evident that as the inclination angle decreases from 180° to 0°, the intensity of flow Ψ_0, Nusselt Number Nu, and Sherwood number Sh initially increase, reaching their peaks at approximately $\Phi \approx 20°$, $\Phi \approx 45°$, and $\Phi \approx 60°$, respectively, before declining. The impact of the power-law index, n, on the stream function, Ψ_0, Nusselt Number Nu, and Sherwood number Sh is depicted in Figures7(1.a)-(1.c), considering values of n ranging from 0.6 to 1.4. Generally, it is observed from Figure 7(1.a) that an increase in n, for a given Φ, notably diminishes the intensity of convective motion. Consequently, both heat and mass transfer rates are significantly impeded with higher values of n, as depicted in Figures 7(1.b) and 7(1.c).

Figures7(2.a)-(2.c) portrays characteristic outcomes for an enclosure exposed to Dirichlet-type boundary conditions. Furthermore, it showcases the influences of the power-law index, n, and the inclination angle, Φ. Analogous to the observations in Figures7(1.a)-(1.c) so that

the peak of the Ψ_0, Nu, and Sh reaching at approximately $\Phi \approx 50°$, $\Phi \approx 40°$, and $\Phi \approx 45°$, respectively, where Neumann boundary conditions are applied, comparable conclusions and insights emerge. Specifically, for shear-thinning fluids ($n < 1$), the magnitudes of the stream function, Ψ_0, Nusselt number, Nu, and Sherwood number, Sh, under Dirichlet-type boundary conditions are notably greater than those under Neumann-type boundary conditions.

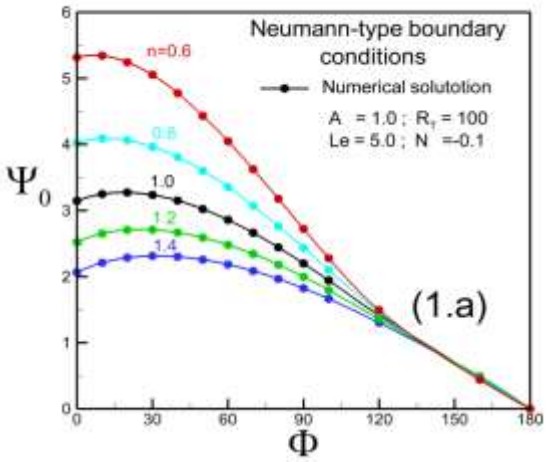
Neumann-type boundary conditions
Numerical solutotion
A = 1.0 ; R_T = 100
Le = 5.0 ; N =-0.1
n=0.6
0.8
1.0
1.2
1.4
Ψ_0
Φ
(1.a)

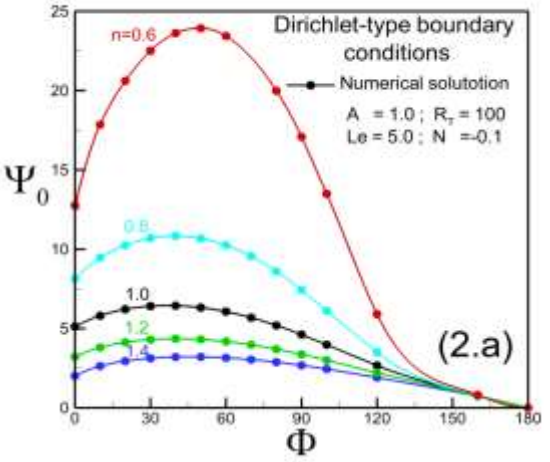
Dirichlet-type boundary conditions
Numerical solutotion
A = 1.0 ; R_T = 100
Le = 5.0 ; N =-0.1
n=0.6
0.8
1.0
1.2
1.4
Ψ_0
Φ
(2.a)

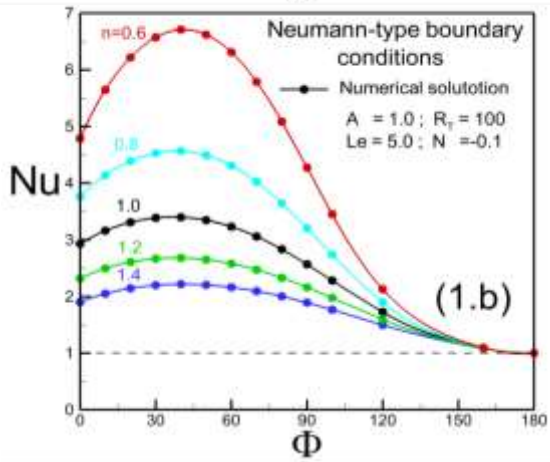
Neumann-type boundary conditions
Numerical solutotion
A = 1.0 ; R_T = 100
Le = 5.0 ; N =-0.1
n=0.6
0.8
1.0
1.2
1.4
Nu
Φ
(1.b)

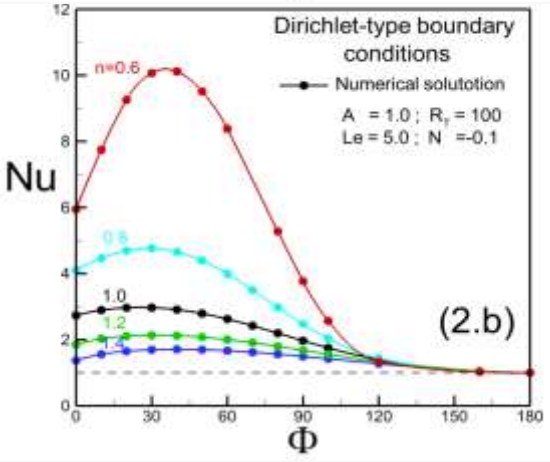
Dirichlet-type boundary conditions
Numerical solutotion
A = 1.0 ; R_T = 100
Le = 5.0 ; N =-0.1
n=0.6
0.8
1.0
1.2
1.4
Nu
Φ
(2.b)

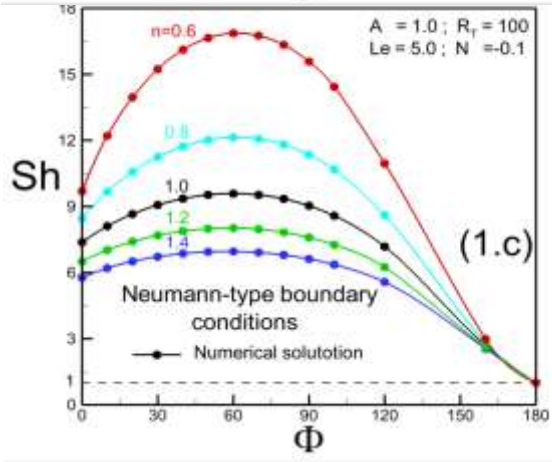
A = 1.0 ; R_T = 100
Le = 5.0 ; N =-0.1
n=0.6
0.8
1.0
1.2
1.4
Sh
Φ
(1.c)
Neumann-type boundary conditions
Numerical solutotion

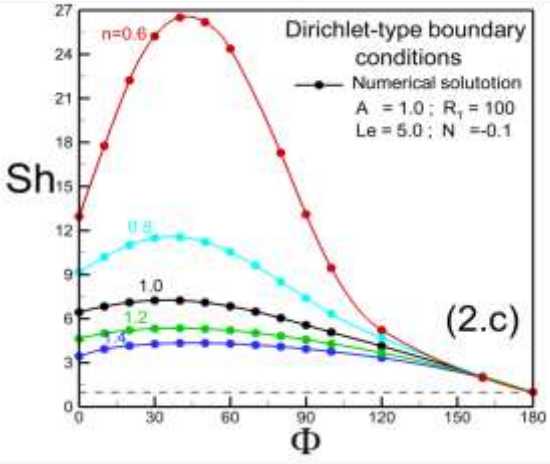
Dirichlet-type boundary conditions
Numerical solutotion
A = 1.0 ; R_T = 100
Le = 5.0 ; N =-0.1
n=0.6
0.8
1.0
1.2
1.4
Sh
Φ
(2.c)

Figure 7.Effects of the inclination angle, Φ, and the power-law index, n, for $R_T = 100$, on: (a) stream function at the center of the cavity Ψ_0, (b) Nusselt number Nu, and (c) Sherwood number Sh. exposed to both Neumann-type (left) and Dirichlet-type (right) boundary conditions.

For $R_T = 100$, $Le = 5$, $\Phi = 90°$, and different values of the power-law index, n, Figures8(a)-(c) depict the influence of the buoyancy ratio, N, on the intensity of flow, Ψ_0, the Nusselt number, Nu, and the Sherwood number, Sh, under Neumann-type boundary conditions. The buoyancy ratio varies between –5 and 5, covering aiding solutal-dominated flow ($N = 5$), fully thermally dominated flow ($N = 0$), and opposed but solutal-dominated flow ($N = -5$). As the power-law index, n, rises, Figures8(a)-(c) illustrate a declining trend in the intensity of flow, the Nusselt number, and Sherwood number for a given value of buoyancy ratio, N. This trend persists irrespectively of aiding or opposing flow. The streamlines depicted in Figure.8(a) reveal that under conditions of simple diffusion (i.e., $N = 0$), convective motion arises solely from temperature gradients, leading to a counter-clockwise thermal circulation ($\Psi_0 > 0$). The flow behavior, as shown in Figure 8(a), is highly dependent on whether the buoyancy ratio is higher or lower than the critical buoyancy ratio, $N_{cr} = -1.2, -1.4, -1.5, -1.5, -1.6$, respectively, for $n = 0.6,0.8,1.0,1.2,1.4$. For these values of N_{cr}, the thermal effects continue to predominate, resulting in Ψ_0 being positive, as shown in Figure 8(d.1). The flow circulation becomes clockwise ($\Psi_0 < 0$) when N is smaller than -1, as indicated by the streamlines in Figure 8(d.2). At this point, the heat and solute buoyant forces are in opposition to one another. It is observed that for values of N between -1 and N_{cr} there is tow stable solution for each value of, n, and there is a transition of flow from counter-clockwise to a clockwise as depicted in Figure 8(d).

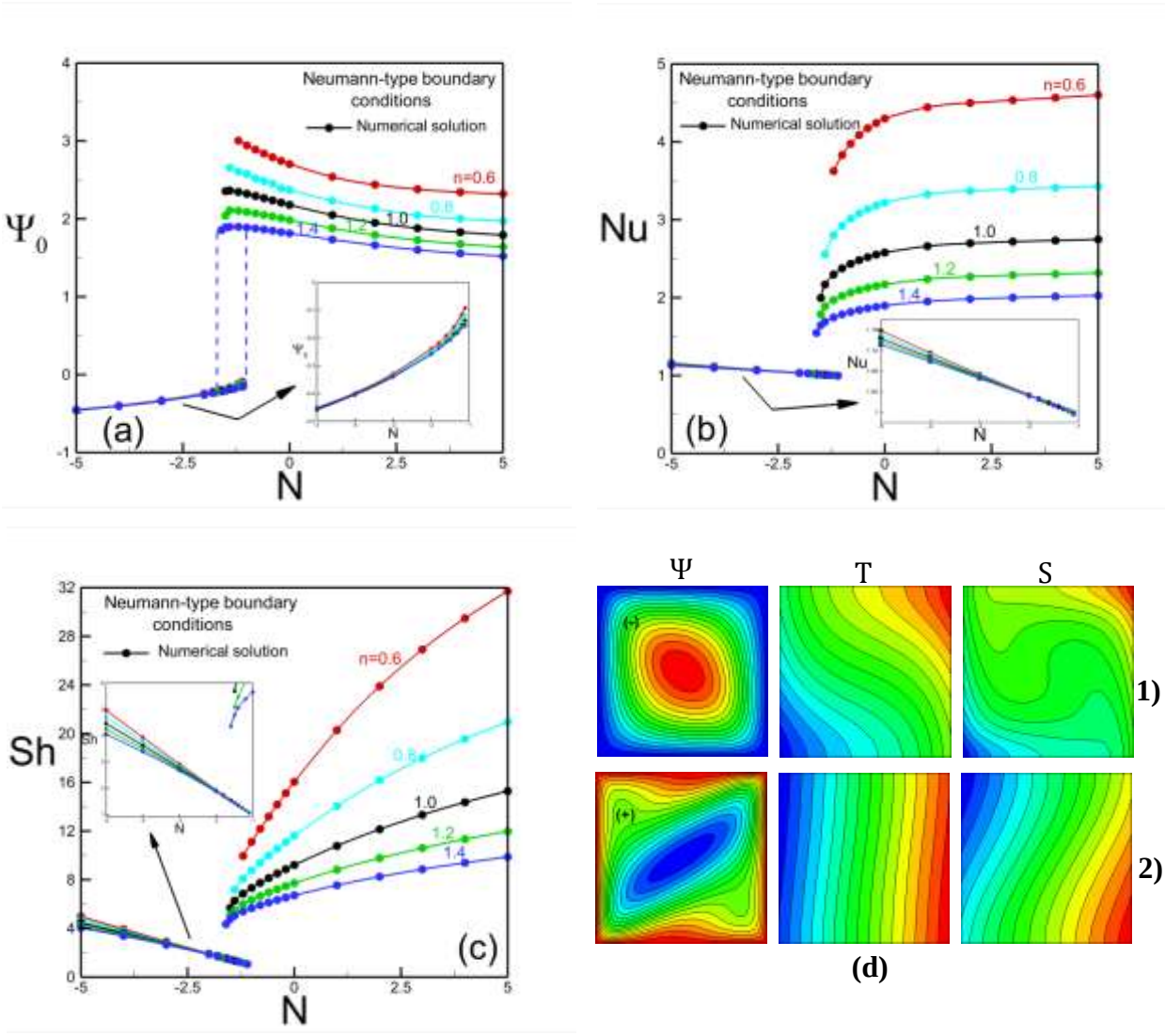

Figure 8. Effects of the buoyancy ratio, Nu, and the power-law index, n, for $R_T = 100$, and $Le = 5$, on: (a) stream function at the centre of the cavity Ψ_0, (b) Nusselt number Nu, and (c) Sherwood number Sh. (d.1) Contours of streamlines, temperature, and concentration for $N = -1.2$, $n = 1.2$: $\Psi_0 = 2.102$, $Nu = 1.968$, and$Sh = 6.005$ (upper solution). (d.2) Contours of streamlines, temperature, and concentration for $N = -1.2$, $n = 1.2$: $\Psi_0 = -1.602$, $Nu = 1.002$, and$Sh = 1.162$, (lower solution) exposed to Neumann-type boundary conditions.

Using the same governing parameters as in Figures8 and 9 illustrates the effects of the buoyancy ratio, N, and the power-law index, n, for a cavity subjected to Dirichlet-type

boundary conditions. Moreover, it is worth noting that each figures contains two curves one start from $N = -0.8$ to 5 which represent a counter-clockwise motion as illustrated by Figures9(a) and 9(d.1), and the other start from $N = -1$ to -5 which represent a clockwise motion as illustrated by Figures9(a) and 9(d.2). It is intriguing to note that for all the values we looked at, the values of flow intensity Ψ_0, Nu, and Sh tend to rise as the absolute values of N grow. It is found that when the power-law index, n, is increased, the strength of fluid movement, the Nusselt number Nu and the Sherwood number Sh, decreases.

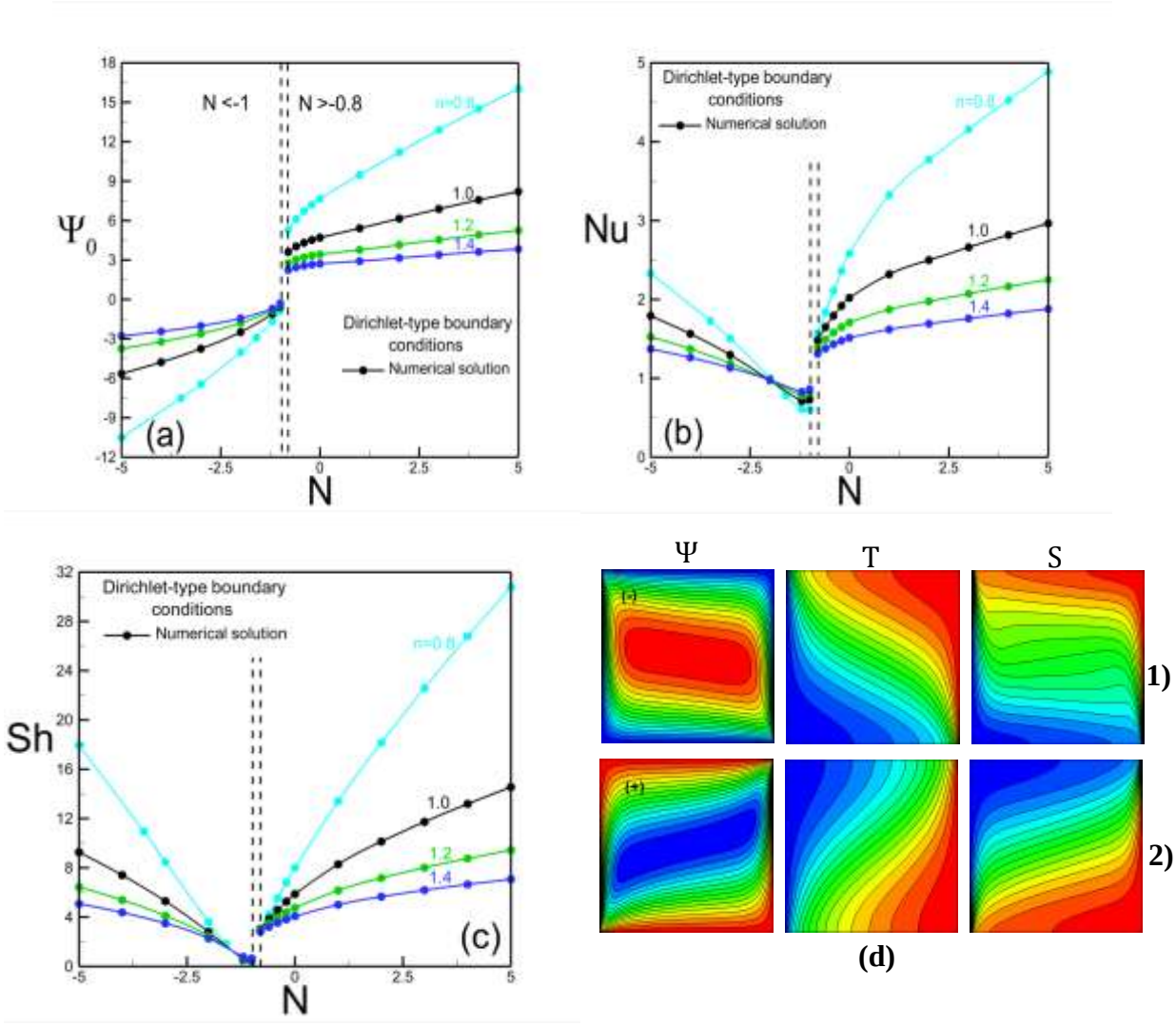

Figure 9. Effects of the buoyancy ratio, N, and the power-law index, n, for $R_T = 100$, and $Le = 5$, on: (a) stream function at the centre of the cavity Ψ_0, (b) Nusselt number Nu, and (c) Sherwood number Sh. (d.1) Contours of streamlines, temperature, and concentration for $N = 3$, $n = 1.2$: $\Psi_0 = 4.541$, $Nu = 2.073$, and $Sh = 8.013$ (right solution). (d.2) Contours of

streamlines, temperature, and concentration for $N = -3$, $n = 1.2$: $\Psi_0 = -2.604$, $Nu = 1.190$, and $Sh = 4.112$, (left solution)exposed to Dirichlet-type boundary conditions.

In the case of shallow enclosures [26], the asymptotic/numerical nonlinear theories' prediction of the convective flow's rheological behavior is highly useful in understanding the shapes of the bifurcation curves and in guiding the investigation of alternative flow configurations, in the absence of asymptotic or analytical solutions. Within this segment, we examine a square enclosure ($A = 1$) that has inflexible bounds. As a result, the outcomes shown below are the predictions of the numerical solution of the full governing equations. Figures 10(a)-(c) depict the numerical outcomes of various convective flow bifurcations (see for instance Khir et al. [26]), presenting flow intensities Ψ_0, Nusselt number Nu, and Sherwood number Sh as functions of R_T under Neumann boundary conditions for distinct values of the power-law index, n. The solid lines in the plots result from a curve fitting process applied to the numerical data, while the dotted-dashed lines are introduced manually to delineate the hypothetical unstable bifurcation branches. As illustrated in Figures 10(a)-(c), the observed trends align qualitatively with prior results reported by Khir et al. [26]. within the context of a shallow enclosure. The flow intensity, Nusselt number, and Sherwood number exhibit a diminishing trend with increasing power-law index. In the case of shear-thinning fluids, the regime consistently remains supercritical. Conversely, for shear-thickening fluids, the bifurcation curves transition from a supercritical behavior to a bi-stability convective state as the power-law index, n, decreases. This behavior is exemplified by the curve shown in the inset of Figure 10(a) for $n = 1.1$, featuring two stable branches connected by an unstable branch (dashed-dotted line). Illustrative representations of streamlines, isotherms, isoconcentrates, and contours of apparent viscosity, acquired for $R_T = 35$, are depicted in Figures 10(d) and (e). Notably, two distinct solutions coexist under identical governing parameter values. The solution portrayed in Figure 10(d), representing the upper stable branch, can be derived by initiating the numerical simulation with finite amplitude flow as initial conditions, following the hysteresis loop denoted by arrows along the bifurcation curves for $n = 1.1$. Conversely, the solution corresponding to the lower stable branch, as shown in Figure 10(e), is attained by commencing the numerical procedure from a pure conduction state as the initial condition.

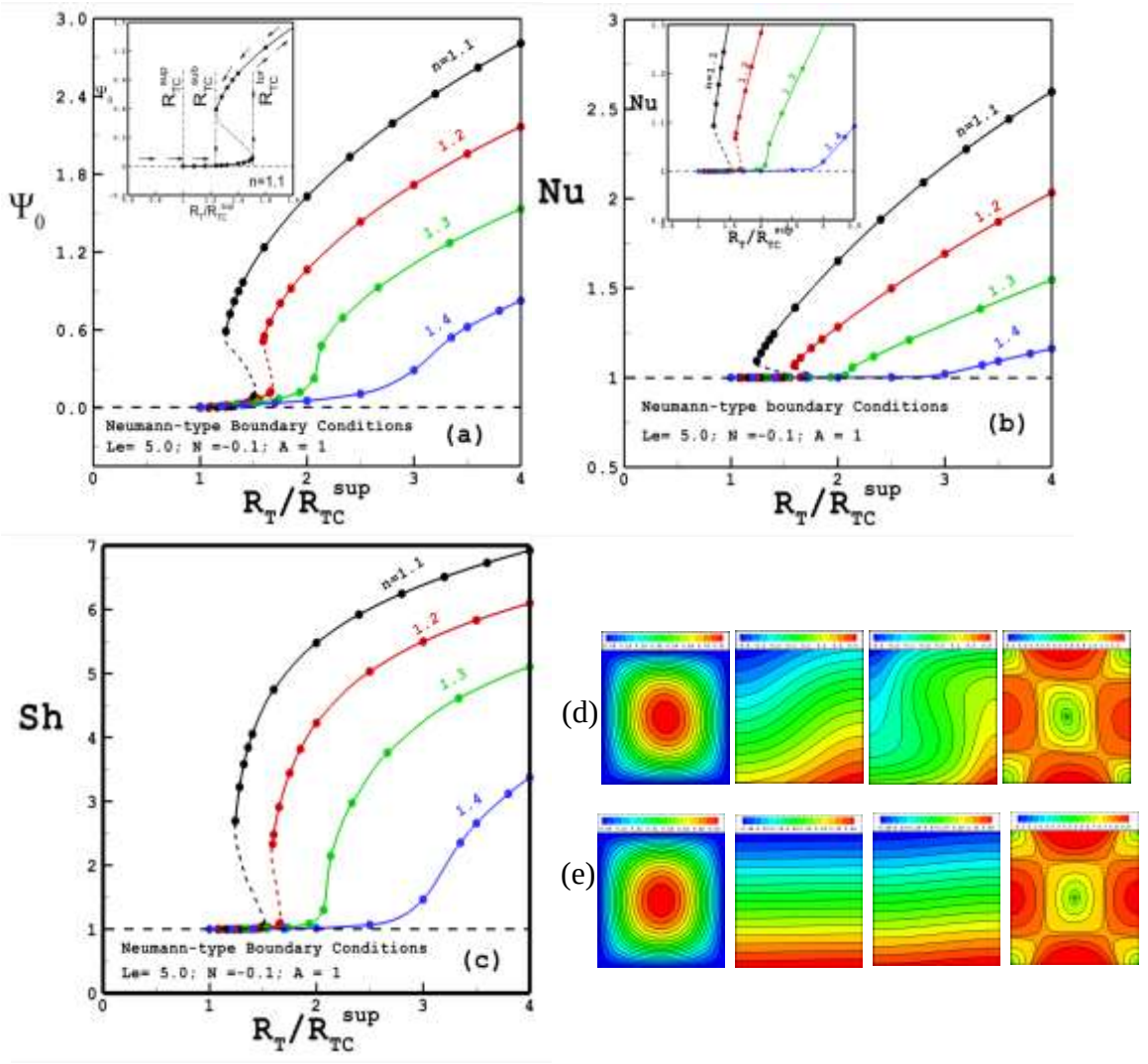

Figure10. Bifurcation diagram in terms of Ψ_0, Nu, and Sh as a function of $R_T$and n for $A = 1$, $Le = 5$, $N = -0.1$: [(a)–(c)] $n = 1.1$ to 1.4.(d) Contours of streamlines, temperature, concentration, and apparent viscosity for$R_T = 35$, $n = 1.1$: $\Psi_0 = 0.9664$, $Nu = 1.2439$, $Sh = 4.0523$, and $\mu_a = 0.4848$ (upper solution). (e) Contours of streamlines, temperature, concentration, and apparent viscosity for $R_T = 35$, $n = 1.1$: $\Psi_0 = 0.0277$, $Nu = 1.0003$, $Sh = 1.0098$, and $\mu_a = 0.3428$ (lower solution) (for Neumann boundary conditions).

Figure 11 presents representative outcomes for an enclosure subjected to Dirichlet-type thermal and solutal boundary conditions, employing the same governing parameters as used in Figure 10. The influence of the shear-thickening effect is also showcased. Similar to the case with Neumann boundary conditions in Figure 10, comparable remarks and observations can be extended to the results, leading to consistent conclusions affirming the presence of bi-

stability convection for Dirichlet thermal and solutal boundary conditions. This affirmation is supported by the bifurcation curves depicted in Figures 11(a)-(c) and the presentation of two distinct numerical solution flow patterns in Figures 11(d)-(e) for $n = 1.1$ and $R_T = 66$. The impact of shear-thickening on bistability convection and heat transfer rate behaviors, as evidenced in both Figures 10 and 11, closely aligns with observations reported for a shallow enclosure with Neumann boundary conditions[26].

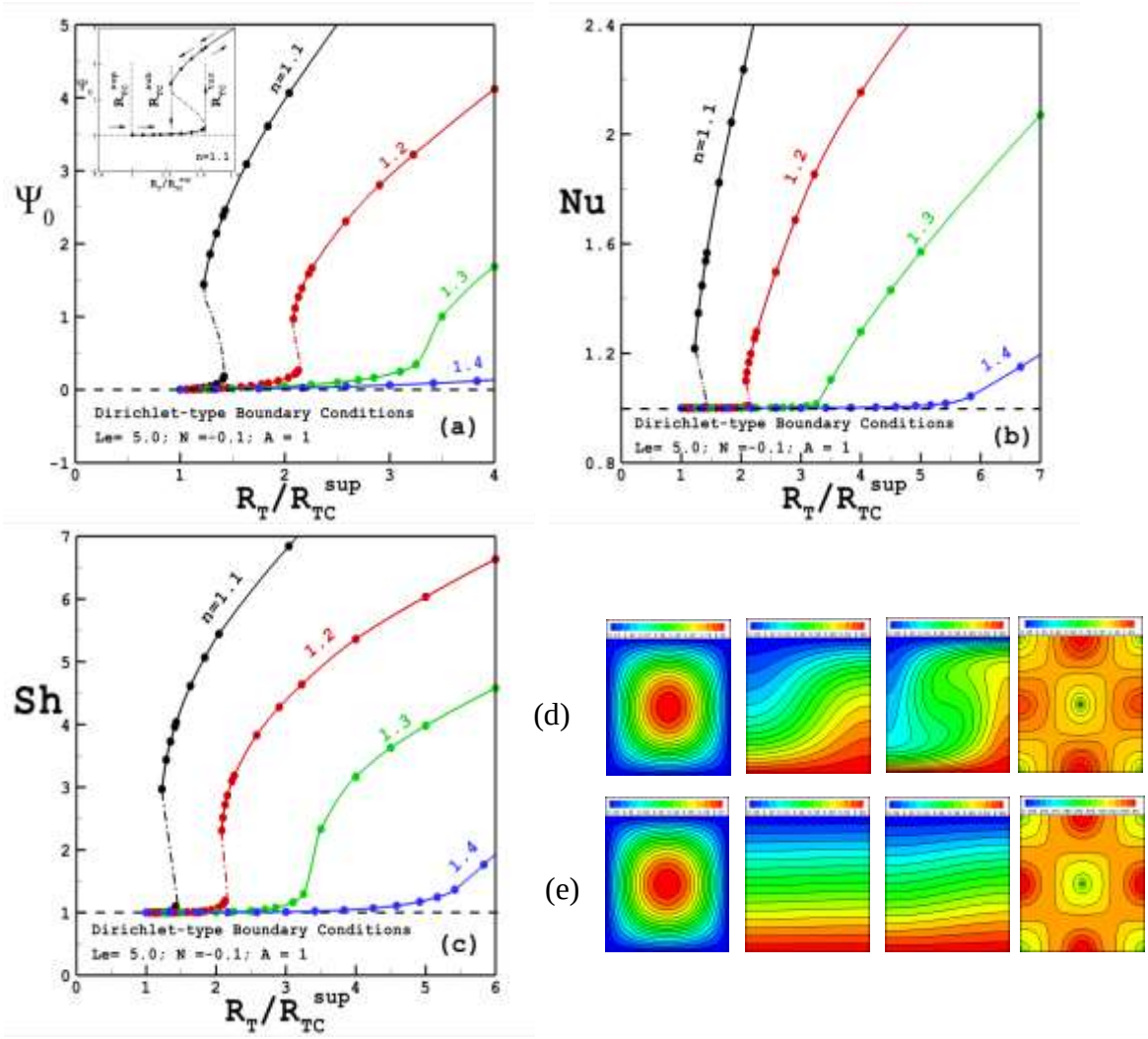

Figure11. Bifurcation diagram in terms of Ψ_0, Nu, and Sh as a function of $R_T$and n for $A = 1$, $Le = 5$, $N = -0.1$: [(a)–(c)] $n = 1.1$ to 1.4.(d) Contours of streamlines, temperature, concentration, and apparent viscosity for$R_T = 66$, $n = 1.1$: $\Psi_0 = 2.1419$, $Nu = 1.4471$, $Sh = 3.7272$, and $\mu_a = 0.4986$ (upper solution). (e) Contours of streamlines, temperature,

concentration, and apparent viscosity for $R_T = 66$, $n = 1.1$: $\Psi_0 = 0.0767$, $Nu = 1.0007$, $Sh = 1.0177$, and $\mu_a = 0.4227$ (lower solution) (for Dirichlet boundary conditions).

Table 3 provides a detailed plot of the critical Rayleigh numbers (R_{TC}^{sub}, R_{TC}^{tur}, and R_{TC}^{sup}) as a function of the power-law index,n, which indicate the onset of motion. This table clearly shows that, under both Neumann-type (left) and Dirichlet-type (right) boundary conditions, the power-law index, n, has a considerable impact on bi-stability convection.

Table.3: Dependence of R_{TC}^{sub}, R_{TC}^{tur} and R_{TC}^{sup} on n for $Le = 5.0$ and $N = -0.1$.

	Neumann-type boundary conditions			**Dirichlet-type boundary conditions**		
$\boldsymbol{n}$	R_{TC}^{sub}	R_{TC}^{tur}	R_{TC}^{sup}	R_{TC}^{sub}	R_{TC}^{tur}	R_{TC}^{sup}
1.1	31	37.6	27	60	69.5	45
1.2	31.8	33.2	18	64.5	66	25
1.3	-	-	12	-	-	16
1.4	-	-	7	-	-	12

VI. CONCLUSIONS

This paper presents a numerical investigation of natural convection with double-diffusive of a non-Newtonian power-law fluid in a saturated porous medium within an inclined square cavity. The study examines the effects under uniform Neumann boundary conditions, featuring constant heat and concentration fluxes, as well as Dirichlet conditions, with constant temperature and concentration. The analysis focuses on the influence of the thermal Rayleigh number,R_T, the power-law index,n, the buoyancy ratio,N, the Lewis number,Le, and the angle of inclination,Φ, on the onset of motion and the rates of heat and mass transfer.

The following briefly describes the primary finding of the current study:

(a) It was found that, for a specific set of governing parameters, the horizontal velocity increases as the power-law index, n, decreases. Conversely, the apparent viscosity, temperature, and concentration decrease with a reduction in n.
(b) A reduction in the power-law index,n, enhances the intensity of convection within the cavity and significantly increases the rate of heat and mass transfer.
(c) Depending on the power law index n and specific values of the governing parameters, the orientation of the cavity has an important effect on the intensity of flow, the heat and mass transfer rates. Regardless of the selected power-law index, n, the highest heat and mass transfer rates under both Neumann-type and Dirichlet-type boundary conditions are observed within the angular ranges of $(10° < \Phi < 70°)$ and $(20° < \Phi < 90°)$, respectively.
(d) The stream function Ψ_0, Nusselt number Nu, and Sherwood number Sh exhibit significantly higher values under Dirichlet-type boundary conditions compared to Neumann-type boundary conditions.

(e) For an inclined cavity with $\Phi = 90°$ (i.e., a vertical cavity), increasing the buoyancy ratio, N, enhances heat and mass transfer due to the dominant buoyancy force. Additionally, the transition from a conductive regime to a convective regime is highly dependent on the power-law index, n, under both Neumann-type and Dirichlet-type boundary conditions.

(f) The phenomenon of bi-stability, characterized by the coexistence of two distinct stable solutions, has been demonstrated in a square cavity under both Neumann-type and Dirichlet-type boundary conditions. This occurrence is notably associated with the properties of dilatant fluids ($n > 1$) and opposing buoyancy forces ($N < 0$).

(g) The power-law index, n, increasingly affected the bi-stability zone. It was discovered that when values of n are increased, the bistability region diminishes and eventually disappears.

REFERENCES

[1] Nield, D. A., & Bejan, A. (2006). Convection in porous media (Vol. 3, pp. 629-982). New York: springer.

[2] Ingham, D. B., & Pop, I. (1998). Transport phenomena in porous media. Elsevier.

[3] Chhabra, R. P., & Richardson, J. F. (1999). Non-Newtonian flow in the process industries: fundamentals and engineering applications. Butterworth-Heinemann.

[4] Hiroyuki, O., Hayatoshi, S., & Churchill, S. W. (1974). Natural convection in an inclined square channel. International Journal of Heat and Mass Transfer, 17(3), 401-406.

[5] Saeid, N. H., & Pop, I. (2005). Non-Darcy natural convection in a square cavity filled with a porous medium. Fluid Dynamics Research, 36(1), 35.

[6] Sarris, I. E., Kakarantzas, S. C., Grecos, A. P., & Vlachos, N. S. (2005). MHD natural convection in a laterally and volumetrically heated square cavity. International Journal of Heat and Mass Transfer, 48(16), 3443-3453.

[7]Pirmohammadi, M., & Ghassemi, M. (2009). Effect of magnetic field on convection heat transfer inside a tilted square enclosure. International Communications in Heat and Mass Transfer, 36(7), 776-780.

[8]Revnic, C., Grosan, T., Pop, I., & Ingham, D. B. (2011). Magnetic field effect on the unsteady free convection flow in a square cavity filled with a porous medium with a constant heat generation. International Journal of Heat and Mass Transfer, 54(9-10), 1734-1742.

[9] Costa, V. A. F., Sousa, A. C. M., & Vasseur, P. (2012). Natural convection in square enclosures filled with fluid-saturated porous media under the influence of the magnetic field induced by two parallel vertical electric currents. International journal of heat and mass transfer, 55(23-24), 7321-7329.

[10]Rebhi, R., Hadidi, N., & Bennacer, R. (2021). Non-Darcian effect on double-diffusive natural convection inside aninclined square Dupuit-Darcy porous cavity under a magnetic field. Thermal Science, 25(1 Part A), 121-132.

[11]Alilat, D., Alliche, M., Rebhi, R., &Borjini, M. N. (2020). Inertial and Porosity Effects on Dupuit-Darcy Natural Convection of Cu-Water Nanofluid Saturated High Thermal Conductive Porous Medium. Special Topics & Reviews in Porous Media: An International Journal, 11(5).

[12]Beghein, C., Haghighat, F., & Allard, F. (1992). Numerical study of double-diffusive natural convection in a square cavity. International Journal of Heat and Mass Transfer, 35(4), 833-846.

[13] Wang, S. C., & Yang, Y. T. (2002). Natural convection of non-Newtonian fluids through permeable axisymmetric and two-dimensional bodies in a porous medium. International Journal of Heat and Mass Transfer, 45(2), 393-408.

[14] Ohta, M., Ohta, M., Akiyoshi, M., & Obata, E. (2002). A numerical study on natural convective heat transfer of pseudoplastic fluids in a square cavity. Numerical Heat Transfer: Part A: Applications, 41(4), 357-372.

[15]Jecl, R., &Škerget, L. (2003). Boundary element method for natural convection in non-Newtonian fluid saturated square porous cavity. Engineering analysis with boundary elements, 27(10), 963-975.

[16] Turan, O., Sachdeva, A., Chakraborty, N., & Poole, R. J. (2011). Laminar natural convection of power-law fluids in a square enclosure with differentially heated side walls subjected to constant temperatures. Journal of Non-Newtonian Fluid Mechanics, 166(17-18), 1049-1063.

[17] Vinogradov, I., Khezzar, L., &Siginer, D. (2012). Heat transfer of non-Newtonian dilatant power law fluids in square and rectangular cavities. Journal of Applied Fluid Mechanics, 4(3), 37-42.

[18] Ahmed, S. E., Hussein, A. K., Mohammed, H. A., Adegun, I. K., Zhang, X., Kolsi, L., ... &Sivasankaran, S. (2014). Viscous dissipation and radiation effects on MHD natural convection in a square enclosure filled with a porous medium. Nuclear Engineering and Design, 266, 34-42.

[19]Kefayati, G. R. (2014). Simulation of non-Newtonian molten polymer on natural convection in a sinusoidal heated cavity using FDLBM. Journal of Molecular Liquids, 195, 165-174.

[20]Astanina, M. S., Sheremet, M. A., &Umavathi, J. C. (2018). Effect of thermal radiation on natural convection in a square porous cavity filled with a fluid of temperature-dependent viscosity. Thermal Science, 22(1 Part B), 391-399.

[21]Astanina, M. S., Sheremet, M. A., &Umavathi, J. C. (2015). Unsteady natural convection with temperature-dependent viscosity in a square cavity filled with a porous medium. Transport in Porous Media, 110, 113-126.

[22]Raisi, A. (2016). The influence of a pair constant temperature baffles on power-law fluids natural convection in a square enclosure. Modares Mechanical Engineering, 15(11), 215-224.

[23]Makayssi, T., Lamsaadi, M., &Kaddiri, M. (2021). Natural double-diffusive convection for the Carreau shear-thinning fluid in a square cavity submitted to horizontal temperature and concentration gradients. Journal of Non-Newtonian Fluid Mechanics, 297, 104649.

[24] Lounis, S., Rebhi, R., Hadidi, N., Lorenzini, G., Menni, Y., Ameur, H., &Sidik, N. A. C. (2022). Thermo-solutal convection of Carreau-Yasuda non-Newtonian fluids in inclined square cavities under Dufour and Soret impacts. CFD Letters, 14(3), 96-118.

[25] Larbi, A. O., Rebhi, R., Rahal, S., Lorenzini, G., Maamar, L., Menni, Y., & Ahmad, H. (2022). Impact of Non-Newtonian Fluids' Rheological Behavior on Double-Diffusive Natural Convection in an Inclined Square Porous Layer. Journal of Advanced Research in Fluid Mechanics and Thermal Sciences, 99(2), 17-47.

[26]Khir, S., Rebhi, R., Kezrane, M., &Borjini, M. N. (2024). Hysteresis and Bistability Bifurcation Induced by Combined Fluid Shear Thickening and Double-Diffusive Convection in Shallow Porous Enclosures Filled with Non-Newtonian Power-Law Fluids. East European Journal of Physics, (1), 203-220.

[27]Khir, S., Rebhi, R., Kezrane, M., Didi, F., & Lounis, S. (2024). Double-diffusive convection of non-Newtonian power-law fluids in an inclined porous layer. Studies in Engineering and Exact Sciences, 5(1), 713-745.

[28]Peaceman, D. W., & Rachford, Jr, H. H. (1955). The numerical solution of parabolic and elliptic differential equations. Journal of the Society for industrial and Applied Mathematics, 3(1), 28-41.